Color Constancy from Hyper-Spectral Data

Th. Gevers, H. M. G. Stokman, J. van de Weijer

Faculty of Science, University of Amsterdam, The Netherlands

{gevers, stokman, joostw}@wins.uva.nl

Abstract

This paper aims for color constant identification of object colors through the analysis of spectral color data. New computational color models are proposed which are not only invariant to illumination variations (color constancy) but also robust to a change in viewpoint and object geometry (color invariance). Color constancy and invariance is achieved by spectral imaging using a white reference, and based on color ratio's (without a white reference). From the theoretical and experimental results it is concluded that the proposed computational methods for color constancy and invariance are highly robust to a change in SPD of the light source as well as a change in the pose of the object.

1 Introduction

Much research in psychology and computer vision has been devoted to the problem of color constancy for discounting the illumination color to obtain the object reflectance color. Color constancy research is extended by the recent object indexing and recognition methods exploring illumination-invariant descriptors from color ratio's and color distributions and significant progress has been achieved. For example, the method proposed by Funt and Finlayson [3] is based on the retinex theory of Land [6] and offers object recognition by indexing on illumination-invariant surface descriptors (color ratios) computed from neighboring points.

While there have been many interesting advances in color constancy, the spectral effect of varying imaging conditions (e.g. a change in camera viewpoint, object pose and shading) and particularly the use of spectral imaging by a spectrograph (as opposed to a spectrophotometer) has not yet been fully explored. Consequently, there is an inevitable need for computational color methods derived from spectral image data which are highly robust to the illumination changes (color constancy) as well as various image-forming parameters such as object shape and camera viewpoint (color invariance).

In this paper, we aim for computational methods for color constant identification of object colors through the analysis of spectral data. We will use an imaging spectrograph which is an instrument capable of simultaneously measuring the optical spectrum components *and* the spatial location of an object surface. In contrast, conventional spectrometers or spectrophotometers are (only) able to measure the optical spectrum from a specific surface area as one point leaving out the spatial information.

The imaging spectrograph provides a spectral range at each pixel covering the UV through NIR (e.g. 400-700nm or 430-900nm). Some advantages of imaging spectroscopy are obvious e.g. very high color measurement precision, no metamerism, spectral color

analysis. In this paper, we will focus on using spectral data for the purpose of color constant identification of object colors. Color constancy is achieved by spectral imaging using a white reference, and based on color ratio's (without a white reference).

This paper is organized as follows. In Section 2, color constancy is discussed using spectral imaging data and a white reference. Further, in Section 3, color constant color ratio's are proposed not only independent of the SPD of the illumination but also robust to a change to object geometry and pose. In Section 4, the two computational color constant methods will be tested for the identification of object colors under varying imaging conditions.

2 Color Constancy and Invariance by Spectral Imaging using a Reference Patch

The spectra obtained by the spectrograph depend on the light source and object characteristics. Therefore, these spectra vary with a change in the intensity and energy distribution of the light source, material characteristics and viewing mode. The aim of this section is to propose spectra which are invariant to illumination (color constancy) and the object geometry and shadows (invariance).

The section is outlined as follows. In Section 2.1, the reflection is modeled as the interaction between light and matter. How to obtain color constant spectra is proposed in Section 2.2. These color constant spectra are further made independent of object geometry and shading (color invariance) in Section 2.3.

2.1 The Reflection Model

Let $E(\vec{x}, \lambda)$ be the spectral power distribution of the incident (ambient) light at the object surface at $\vec{x}$, and let $L(\vec{x}, \lambda)$ be the spectral reflectance function of the object at $\vec{x}$. The spectral sensitivity of the kth sensor is given by $F_k(\lambda)$. Then ρ_k, the sensor response of the kth channel, is given by:

$$\rho_k(\vec{x}) = \int_\lambda E(\vec{x}, \lambda) L(\vec{x}, \lambda) F_k(\lambda) d\lambda \tag{1}$$

where λ denotes the wavelength, and $L(\vec{x}, \lambda)$ is a complex function based on the geometric and spectral properties of the object surface. The integral is taken from the visible spectrum (e.g. 400-700 nm).

Further, consider an opaque inhomogeneous dielectric object having diffuse reflection (i.e. matte surface), then the geometric and surface reflection components of function $L(\vec{x}, \lambda)$ can be modeled by the (diffuse) body reflection described by Shafer [9]:

$$\phi_k(\vec{x}) = G_B(\vec{x}, \vec{n}, \vec{s}) \int_\lambda E(\vec{x}, \lambda) B(\vec{x}, \lambda) F_k(\lambda) d\lambda \tag{2}$$

giving the kth sensor response. Further, $B(\vec{x}, \lambda)$ is the surface albedo at $\vec{x}$. $\vec{n}$ is the surface patch normal, and $\vec{s}$ is the direction of the illumination source. Geometric term G_B denotes the geometric dependency on the reflection.

2.2 Color Constancy

Consider the reflectance of a perfect reflecting white diffuser. A sample is called a perfect white when the sample diffusely reflects all wavelengths of the light source and does not absorb any of them. Diffuse reflectance implies that the reflected light is symmetrical in all directions. The white diffuser used in this paper is a Spectralon white reference tile with a spectral reflectance ratio [5] of over 0.990 ± 0.001 in the visible wavelength range. Hence, we may assume that the white diffuser has spectral albedo reflectance $B^w(\lambda) = 0.990$. Further, having diffuse reflectance and assuming that the surface normal $\vec{n}$ is equal to the viewing direction $\vec{s}$, then $G_B(\vec{x}, \vec{n}, \vec{s}) = 1$. Then the sensor response of the kth channel of the matte white reference sample is given by:

$$\phi_k^w(\vec{x}) = \int_\lambda E(\vec{x}, \lambda) F_k(\lambda) B^w(\lambda) d\lambda \tag{3}$$

In this way, the relative spectral power distribution of the white reference is measured.

Further, a spectral image is captured of an arbitrary sample under the same illumination conditions, and the image is divided by the previously obtained recording of the illuminant. We thus have:

$$\frac{\phi_k(\vec{x})}{\phi_k^w(\vec{x})} = \frac{G_B(\vec{x}, \vec{n}, \vec{s}) \int_\lambda E(\vec{x}, \lambda) B(\vec{x}, \lambda) F_k(\lambda) d\lambda}{\int_\lambda E(\vec{x}, \lambda) F_k(\lambda) B^w(\lambda) d\lambda} \tag{4}$$

giving the kth sensor response of a sample with respect to a white reference. Through the use of the spectrograph, the filters $F_k(\lambda)$ are narrow-band filters. Let the filter $F_k(\lambda)$ be modeled as a unit impulse that is shifted over N wavelengths: the transmission at $\lambda_k = \delta$ and zero elsewhere. This allows us to rewrite equation (4) as:

$$\frac{\phi_k(\vec{x})}{\phi_k^w(\vec{x})} = \frac{G_B(\vec{x}, \vec{n}, \vec{s}) E(\vec{x}, \lambda_k) B(\vec{x}, \lambda_k)}{E(\vec{x}, \lambda_k) B^w(\lambda_k)} \tag{5}$$

obtaining:

$$\frac{\phi_k(\vec{x})}{\phi_k^w(\vec{x})} = \frac{G_B(\vec{x}, \vec{n}, \vec{s}) B(\vec{x}, \lambda_k)}{B^w(\lambda_k)} \tag{6}$$

Eq. 6 implies that, under the assumption of a unit impulse band filter, the observed spectra can be made independent of the actual spectral distribution of the light source and be made independent of the spatial variance of the intensity of the illuminant, if the original image is divided by the white reference image. As $B_w(\lambda)$ is known from the calibrated white reference, the true fraction of light $B(\vec{x}, \lambda)$ reflected at a certain wavelength at position $\vec{x}$ is obtained by

$$B(x, \lambda) = \frac{\phi_k(\vec{x})}{\phi_k^w(\vec{x})} \cdot B^w(\lambda) \tag{7}$$

Note that the spectral power distribution of the light source is unimportant as long as it contains all wavelengths of the visible light in a sufficient amount.

2.3 Invariance

In this section, the color constant spectra are normalized yielding spectra which are independent of the object geometry.

Let us rewrite equation (6) as:

$$D_k(\vec{x}) = \frac{\phi_k(\vec{x})}{\phi_k^w(\vec{x})} = G_B(\vec{x}, \vec{n}, \vec{s}) \frac{B(\vec{x}, \lambda_k)}{B^w(\lambda_k)} \tag{8}$$

According to equation (8), the color itself depends only on surface albedo whereas the brightness of the color depends on factor $G_B(\vec{x}, \vec{n}, \vec{s})$. As a consequence, a uniformly painted surface may give rise to a broad variance of sensor values due to a change in object geometry.

In contrast, normalized sensor space is insensitive to surface orientation, illumination direction and intensity by the division of each channel by the sum of channels:

$$C_k(\vec{x}) = \frac{D_k(\vec{x})}{D_1(\vec{x}) + D_2(\vec{x}) + ... + D_N(\vec{x})} =$$

$$\frac{G_B(\vec{x}, \vec{n}, \vec{s}) B(\vec{x}, \lambda_k)}{G_B(\vec{x}, \vec{n}, \vec{s})(B(\vec{x}, \lambda_1) + B(\vec{x}, \lambda_2) + ... + B(\vec{x}, \lambda_N))} =$$

$$\frac{B(\vec{x}, \lambda_k)}{B(\vec{x}, \lambda_1) + B(\vec{x}, \lambda_2) + ... + B(\vec{x}, \lambda_N)} \tag{9}$$

Thus, normalized sensor space only dependent on the surface albedo and is invariant of the illumination spectral power distribution, illumination direction $\vec{s}$, and object geometry $\vec{n}$.

3 Color Constancy and Invariance by Spectral Imaging using Color Ratio's

Most color constancy methods require specific a priori information about the observed scene [2], [6] for example. To circumvent these problems, simple and effective illumination-independent color ratio's have been proposed by Funt and Finlayson [3] and Nayar and Bolle [7]. In fact, these color models are based on the ratio of surface albedos rather then the recovering of the actual surface albedo itself. However, these color models assume that the variation in spectral power distribution of the illumination can be modeled by the coefficient rule or von Kries model, where the change in the illumination color is approximated by a 3x3 diagonal matrix among the sensor bands and is equal to the multiplication of each RGB-color band by an independent scalar factor. The diagonal model does not hold in general. However, the diagonal model of illumination change holds exactly in the case of narrow-band sensors. In this paper, through the use of the spectrograph, the filters $F_k(\lambda)$ are essentially narrow-band filters.

Consider the body reflection term of the dichromatic reflection model with narrow-band filters:

$$C_k(\vec{x}) = G_B(\vec{x}, \vec{n}, \vec{s}) E(\vec{x}, \lambda_k) B(\vec{x}, \lambda_k) \tag{10}$$

giving the measured sensor pulse response of a matte infinitesimal surface patch of an inhomogeneous dielectric object under unknown spectral power distribution of the illumination.

The color ratio's proposed by Nayar and Bolle is given by [7]:

$$N(C^{\vec{x}_1}, C^{\vec{x}_2}) = \frac{C^{\vec{x}_1} - C^{\vec{x}_2}}{C^{\vec{x}_2} + C^{\vec{x}_1}} \tag{11}$$

and by Funt and Finlayson by [3]:

$$F(C^{\vec{x}_1}, C^{\vec{x}_2}) = \frac{C^{\vec{x}_1}}{C^{\vec{x}_2}} \tag{12}$$

expressing color ratio's between two neighboring image locations, for $C \in \{C_1, C_2, ..., D_N\}$, where $\vec{x}_1$ and $\vec{x}_2$ denote the image locations of the two neighboring pixels. Note that C_k are measured colors with narrow-band sensor filters. Note that standard digital camera's are not equipped with narrow-band filters. In this paper, the spectral images obtained by the spectrograph are essentially narrow-band filters.

Assuming that the color of the illumination is locally constant (i.e. $E(\vec{x}_1, \lambda_k) = E(\vec{x}_2, \lambda_k)$) and that neighboring points have the same surface orientation (i.e. $G_B(\vec{x}_1, \vec{n}, \vec{s}) = G_B(\vec{x}_2, \vec{n}, \vec{s})$), then the color ratio N is independent of the illumination intensity and color as shown by substituting equation (10) in equation (11):

$$N(C^{\vec{x}_1}, C^{\vec{x}_2}) = \frac{C^{\vec{x}_1} - C^{\vec{x}_2}}{C^{\vec{x}_2} + C^{\vec{x}_1}} =$$

$$\frac{G_B(\vec{x}_1, \vec{n}, \vec{s})E(\vec{x}_1, \lambda_k)B(\vec{x}_1, \lambda_k) - G_B(\vec{x}_2, \vec{n}, \vec{s})E(\vec{x}_2, \lambda_k)B(\vec{x}_2, \lambda_k)}{G_B(\vec{x}_1, \vec{n}, \vec{s})E(\vec{x}_1, \lambda_k)B(\vec{x}_1, \lambda_k) + G_B(\vec{x}_2, \vec{n}, \vec{s})E(\vec{x}_2, \lambda_k)B(\vec{x}_2, \lambda_k)} =$$

$$\frac{B(\vec{x}_1, \lambda_k) - B(\vec{x}_2, \lambda_k)}{B(\vec{x}_1, \lambda_k) + B(\vec{x}_2, \lambda_k)} \tag{13}$$

Equal arguments hold for the color ratio F by substituting equation (10) in equation (12):

$$F(C^{\vec{x}_1}, C^{\vec{x}_2}) = \frac{C^{\vec{x}_1}}{C^{\vec{x}_2}} = \frac{G_B(\vec{x}_1, \vec{n}, \vec{s})E(\vec{x}_1, \lambda_k)B(\vec{x}_1, \lambda_k)}{G_B(\vec{x}_2, \vec{n}, \vec{s})E(\vec{x}_2, \lambda_k)B(\vec{x}_2, \lambda_k)} = \frac{B(\vec{x}_1, \lambda_k)}{B(\vec{x}_2, \lambda_k)} \tag{14}$$

However, it is assumed that the neighboring points, from which the color ratio's are computed, have the same surface normal. Therefore, the method depends on varying surface orientation of the object (i.e. the geometry of the objects) affecting negatively the recognition performance. To this end, a new color constant color ratio is proposed not only independent of the illumination color but also discounting the object's geometry:

$$M(C_1^{\vec{x}_1}, C_1^{\vec{x}_2}, C_2^{\vec{x}_1}, C_2^{\vec{x}_2}) = \frac{C_1^{\vec{x}_1}C_2^{\vec{x}_2} - C_1^{\vec{x}_2}C_2^{\vec{x}_1}}{C_1^{\vec{x}_2}C_2^{\vec{x}_1} + C_1^{\vec{x}_1}C_2^{\vec{x}_2}}, C_1 \neq C_2 \tag{15}$$

expressing the color ratio between two neighboring image locations, for $C_1, C_2 \in \{C_1, C_2, ..., D_N\}$ where $\vec{x}_1$ and $\vec{x}_2$ denote the image locations of the two neighboring pixels.

The color ratio is independent of the illumination intensity and color, and also to a change in viewpoint, object geometry, and illumination direction as shown by substituting equation (10) in equation (15):

$$M(C_1^{\vec{x}_1}, C_1^{\vec{x}_2}, C_2^{\vec{x}_1}, C_2^{\vec{x}_2}) = \frac{C_1^{\vec{x}_1}C_2^{\vec{x}_2} - C_1^{\vec{x}_2}C_2^{\vec{x}_1}}{C_1^{\vec{x}_2}C_2^{\vec{x}_1} + C_1^{\vec{x}_1}C_2^{\vec{x}_2}}, C_1 \neq C_2$$

$$\frac{(G_B(\vec{x_1},\vec{n},\vec{s})E(\vec{x_1},\lambda_k)B(\vec{x_1},\lambda_{C_1}))(G_B(\vec{x_2},\vec{n},\vec{s})E(\vec{x_2},\lambda_k)B(\vec{x_2},\lambda_{C_2}))-}{(G_B(\vec{x_2},\vec{n},\vec{s})E(\vec{x_2},\lambda_k)B(\vec{x_2},\lambda_{C_1}))(G_B(\vec{x_1},\vec{n},\vec{s})E(\vec{x_1},\lambda_k)B(\vec{x_1},\lambda_{C_2}))+}$$

$$\frac{(G_B(\vec{x_2},\vec{n},\vec{s})E(\vec{x_2},\lambda_k)B(\vec{x_1},\lambda_{C_1}))(G_B(\vec{x_1},\vec{n},\vec{s})E(\vec{x_1},\lambda_k)B(\vec{x_1},\lambda_{C_2}))}{(G_B(\vec{x_1},\vec{n},\vec{s})E(\vec{x_1},\lambda_k)B(\vec{x_1},\lambda_{C_1}))(G_B(\vec{x_2},\vec{n},\vec{s})E(\vec{x_2},\lambda_k)B(\vec{x_2},\lambda_{C_2}))} =$$

$$\frac{B(\vec{x_1},\lambda_{C_1})B(\vec{x_2},\lambda_{C_2}) - B(\vec{x_2},\lambda_{C_1})B(\vec{x_1},\lambda_{C_2})}{B(\vec{x_2},\lambda_{C_1})B(\vec{x_1},\lambda_{C_2}) + B(\vec{x_1},\lambda_{C_1})B(\vec{x_2},\lambda_{C_2})} \tag{16}$$

factoring out dependencies on object geometry and illumination direction $G_B(\vec{x_1},\vec{n},\vec{s})$ and $G_B(\vec{x_2},\vec{n},\vec{s})$, and illumination for $E(\vec{x_1},\lambda_{C_2})) = E(\vec{x_2},\lambda_{C_2})$, and hence only dependent on the ratio of surface albedos, where $\vec{x_1}$ and $\vec{x_2}$ are two neighboring locations on the object's surface not necessarily of the same orientation.

Note that the color ratio's do not require any specific a priori information about the observed scene, as the color model is an illumination-invariant surface descriptor based on the ratio of surface albedos rather then the recovering of the actual surface albedo itself. Also the intensity and spectral power distribution of the illumination is allowed to vary across the scene (e.g. multiple light sources with different SPD's), and a certain amount of object occlusion and cluttering is tolerated due to the local computation of the color ratio.

4 Experiments

Unless stated differently, all experiments are performed using a Jain CV-M300 monochrome CCD camera, Matrox Corona Frame-grabber, Navitar 7000 zoom lens, Spectalon white reference, Imspector V7 spectrograph, 500 Watt halogen illumination and the MacBeth ColorChecker. The spatial resolution is 40 μm per pixel, the exposure time of the 8-bits camera is 1/25 second per frame.

In Section 4.1, experiments are described that study the spectrograph output by comparison with calibrated standards. In Section 4.2, experiments are conducted to evaluate the stability of the different color ratio's with respect to a change in illumination spectral power distribution, object geometry and a change in object pose.

4.1 Color Constancy by Spectral Imaging using a White Reference

If twice as much light enters the camera, then a twice as high (linear) camera output is expected. If no light enters the camera, then zero camera output is expected. Calibration assures these assumptions. Furthermore, it is determined which row at the CCD grid corresponds to which wavelength, and by using calibrated standards it is determined which gray value corresponds to which percentage of reflection.

Photometric scale calibration The camera lens is covered with a dark sheet which contains a small hole with radius of approximately 0.5 cm. Two halogen light sources are used to illuminate the white reference. Three recordings of the white reference are made: One recording when the white reference is illuminated by one illuminant, the second recording when the reference is illuminated by the second illuminant, and the third recording using both illuminants. Invariably, the three recordings show a small, bright circle with varying intensity. The average brightness value is computed over the circle for the three images
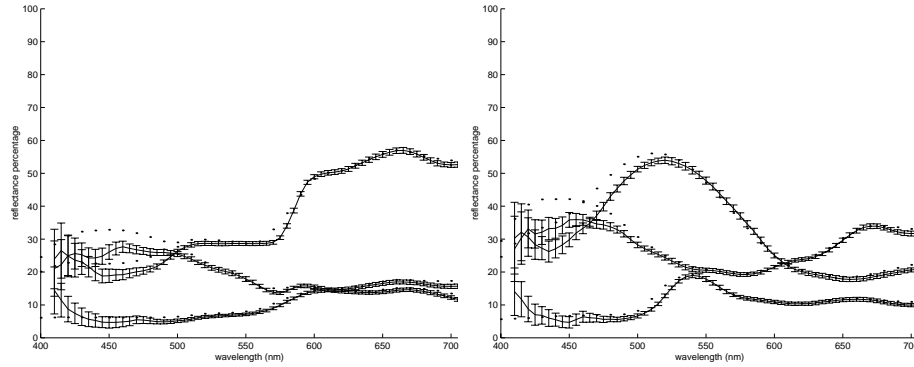
Figure 1: *Experiment: Comparison of the spectrograph with a spectrophotometer. Left: Color patches 1 (dark skin), 2 (light skin) and 3 (blue sky). Right: Color patches 4 (foliage), 5 (blue flower) and 6 (bluish green). Error bars denote the standard deviation of the average reflectance percentage measured by the Imspector V7 spectrograph. Dotted lines denote the reflectance percentage measured by X-Rite SP78 spectrophotometer.*

over $N \approx 15,000$ pixels. The values are 104 ± 4, 123 ± 4 for the two singly illuminated circles and 219 ± 6 for the doubly illuminated circle, respectively. The dark current is measured as 6 ± 1 in the scale of $0 \cdots 255$. After correction for the dark current, the discrepancy is less than one percent and it is concluded that the camera output is linear.

Wavelength calibration For the experiment, narrow bandpass filters are used which transmit at 50-nm intervals in the visible wavelength range. They have a transmittance of 10-nm bandwidth around their bandpass wavelength [8]. The filters are placed in front of the camera lens and an image is captured of a white sample. The aperture is adjusted for each filter to obtain a maximal signal. The position at the optical axis of the line corresponds to the transmitted wavelength of the filter. A low sensitivity of the CCD camera is seen for lower wavelengths. Estimation of the bandpass wavelength is done by convolution with a one-dimensional Gauss filter with $\sigma = 10$ pixels. The results are averaged over the spatial axis. The rows corresponding to 5-nm intervals are obtained by linear interpolation from the results. The table shows that the minimal distance between two consecutive (50-nm apart) bandpass filters is 89.3 pixels. Our interest is in a spectral resolution of 5-nm. The width of the filter is therefore $K = 89.3/10 = 9$ pixels sufficient for our purposes.

Comparison of the Spectrograph with a Spectrophotometer For this experiment, the MacBeth ColorChecker, the Jain camera and Imspector V7, and a X-Rite SP78 Sphere Spectrophotometer are used. The spectrophotometer samples the visible wavelength at 10 nm intervals. Goal of the experiment is to compare the reflectance percentages measured by the spectrograph with that of the spectrophotometer. The reflectance that are compared are in the range of $410 \cdots 700$ nm, the wavelength interval is 10 nm. The differences in reflectances are shown in Figures 1 and 2. The average difference in the reflection percentage is $\overline{\%R} = 2.0 \pm 0.7$. Assuming a normal distribution of the average difference in
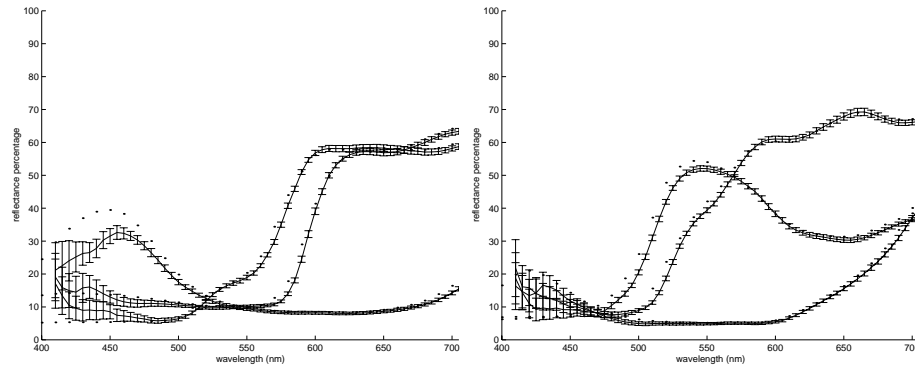
Figure 2: *Experiment: Comparison of the spectrograph (error bars) with a spectropho-tometer (dots). Left: Color patches 7 (orange), 8 (purplish blue) and 9 (moderate red). Right: Color patches 10 (purple), 11 (yellow green) and 12 (orange yellow).*

the reflection percentage, the experiment shows that the difference in reflectance percent-age between the spectrograph and a spectrophotometer is less than 5%.

4.2 Color Constancy by Spectral Imaging using Color Ratio's

In this section, experiments are conducted to evaluate the stability of the different color ratio's with respect to a change in illumination spectral power distribution, object geometry and a change in object pose. As the color ratio's proposed by Nayar and Finlayson are similar, we focus on the color ratio's of Nayar and the color ratio M proposed in this paper.

To test the robustness of the color ratio's with respect to a change in spectral power distribution of the light source, the MacBeth ColorChecker has been recorded by the spec-trograph under the following light sources: (1) an incandescent lamp of about 2900 K (2) a fluorescent lamp of about 4100 K (3) a halogen lamp of about 6500 K. Note that the MacBeth ColorChecker is flat and that differences in the measured color are only due to a change in SPD of the light source illuminating the samples. In Figure 3, the color ratio's differentiated for the various wavelengths have been computed for two colors of the Mac-Beth ColorChecker under the three different light sources. It can be seen that the color ratio's of N and M gave similar results and are robust against a change in SPD. We have further tested the color ratio's on the 18 colored samples of the MacBeth ColorChecker. The squared error between the color ratio's over the wavelengths yielded a total average error of 2.4% for N and 2.8% for M over the total range yielding excellent results for both N and M.

In order to evaluate the different color ratio's with respect to a change in geometry, images have been taken by the spectrograph from 3D matte man-made objects. Note that, in theory, the color ratio N depends on varying surface orientation of the object (i.e. the geometry of the objects). Further, M is robust to a change in object geometry and illu-mination direction. Thirty matte and homogeneously colored objects were used in the ex-periments. The objects were put in front of the spectrograph. The thirty recordings were made under the same light source. Then the same thirty objects were recorded again un-der the same light source but this time with a new, arbitrary position and orientation with
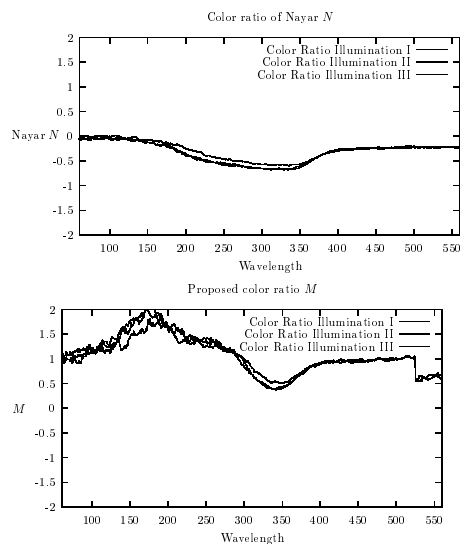
Figure 3: *Experiment: Evaluating the robustness of the color ratio's with respect to a change in SPD of the light source. Top: Nayar color ratio N computed over the wavelengths taken from two colors of the MacBeth ColorChecker recorded by the Imspector V7 spectrograph under three different light sources. Down: Proposed color ratio M computed over the wavelengths taken from two colors of the MacBeth ColorChecker recorded by the Imspector V7 spectrograph under three different light sources.*
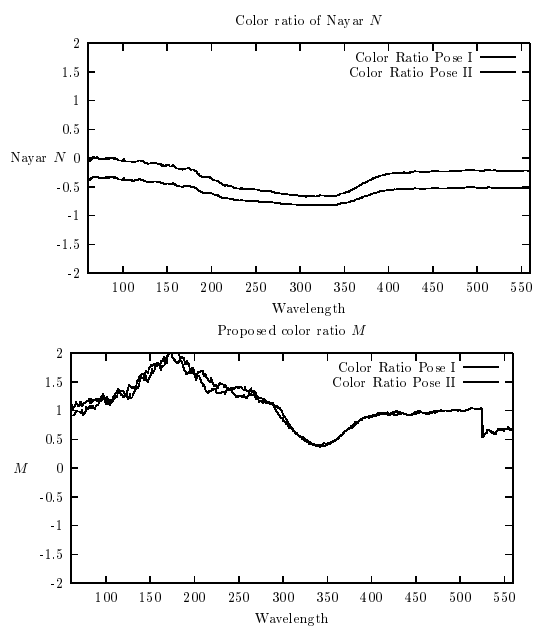

Figure 4: *Experiment: Evaluating the robustness of the color ratio's with respect to a change in object pose. Top: Nayar color ratio N computed over the wavelengths taken from two colors from the MacBeth ColorChecker recorded by the Imspector V7 spectrograph under the same light source but under different poses. Down: Proposed color ratio M computed over the wavelengths taken from two colors from the MacBeth ColorChecker recorded by the Imspector V7 spectrograph under the same light source but under different poses.*

respect to the camera, some recorded upside down, some rotated, some at different distances. An example result is shown in Figure 4, where two recordings are made of the same MacBeth ColorChecker color sample but under different orientations with respect to the spectrograph. The color ratio's have been recorded over the wavelength for N and M. It can easily be seen that N is heavily dependent on the geometry and pose of the object whereas M is relatively stable. The average error between the color ratio's differentiated for the 30 objects resulted in 20% for N and only 3.4% for M of the total range of the color ratio values. In conclusion, M is highly robust to a change in SPD of the light source as well as a change in the pose of the object. Further, N is only robust to a change in SPD of the light source.

5   Conclusion

This paper presented computational methods for color constant identification of object colors through the analysis of spectral color data. Color constancy has been achieved by spectral imaging using a white reference, and based on color ratio's (without a white reference). From the theoretical and experimental results it is concluded that the proposed color constant methods are highly robust to a change in SPD of the light source as well as a change in the pose of the object.

References

[1] Finlayson, G.D., Drew, M.S., and Funt, B.V., *Spectral Sharpening: Sensor Transformation for Improved Color Constancy*, JOSA, 11, pp. 1553-1563, May, 1994.

[2] Forsyth, D., *A Novel Algorithm for Color Constancy*, International Journal of Computer Vision, Vol. 5, pp. 5-36, 1990.

[3] Funt, B. V. and Finlayson, G. D., *Color Constant Color Indexing*, IEEE PAMI, 17(5), pp. 522-529, 1995.

[4] T. Gevers and Arnold W.M. Smeulders, *Content-based Image Retrieval by Viewpoint-invariant Image Indexing*, Image and Vision Computing, (17)7, 1999.

[5] Labsphere Inc., Reflectance Calibration Laboratory. *Calibration Certificate*, September 1998. Spectralon Reflectance Target, Sample I.D.: SRT-99-050.

[6] E. H. Land and J. J. McCann, Lightness and Retinex Theory, *J. Opt. Soc. Am.* **61**, 1-11, (1971).

[7] S. K. Nayar, and R. M. Bolle, Reflectance Based Object Recognition, International Journal of Computer Vision, Vol. 17, No. 3, pp. 219-240, 1996

[8] Orion Corp. *Technical Data*, October 1998. Filters s10_400s, s10_450s, s10_500s, s10_550s, s10_600s, s10_650s, s10_700s.

[9] Shafer, S. A., *Using Color to Separate Reflection Components*, COLOR Res. Appl., 10(4), pp 210-218, 1985.